

# 3-D Unsteady Computational Studies of a Four-Fin Bio-Inspired UUV

Ravi Ramamurti<sup>1</sup>, Jason Geder<sup>1</sup>,  
John Palmisano<sup>2</sup>, Marius Preussner<sup>2</sup>,  
Banahalli Ratna<sup>2</sup> and William Sandberg<sup>3</sup>

<sup>1</sup> *Laboratory for Computational Physics and Fluid Dynamics,*

<sup>2</sup> *Center for Bio-molecular Science and Engineering*  
Naval Research Laboratory, Washington, D.C., 20375.

<sup>3</sup> *Modeling and Analysis Division,*  
Science Applications Intl. Corp. McLean, VA 22102.

## Abstract

The development of an unmanned underwater vehicle (UUV) with four actively controlled curvature flapping fins is described. Three dimensional unsteady flow computations past several configuration of the vehicle are computed and based on the minimum drag a nearly elliptical cross-section with a smooth leading and trailing sections was obtained. The hydrodynamic characteristics of this vehicle at NRL are computed for a range of operational conditions and a dynamic mode of this vehicle was created for the development of a controller. Detailed parametric studies were carried out varying several physical and kinematic parameters, such as separation of the two fins, the phasing of the rear fin with respect to the front fin, the vehicle speed, and the fin orientation. The unsteady flow solver is coupled to a 6-dof model to simulate an unconstrained yaw maneuver of the vehicle.

## I. Introduction

Current unmanned underwater vehicles (UUVs) operate with propellers and conventional control surfaces and are designed for cruise. These are not well suited for operating in cluttered, near shore environments where maneuvering and controllability at low speed, unsteady flow are important. Flapping and deforming fins may provide significant low-speed maneuvering, obstacle avoidance and position keeping capabilities for future UUV operations. Oscillatory deforming wing and fin motion for propulsive force generation is common in birds and fishes but uncommon in man-made vehicles. This mode of propulsion, which also might not need body undulation, has many applications, such as submersibles propulsion, maneuvering, and flow control. These are of interest to the UUV hydrodynamic community and the aerodynamic community for the study of unconventional aerodynamics of Micro Aerial Vehicles (MAV) and aircraft flutter. We address the question here of the importance of flapping surface deformation to the magnitude of propulsive force generation.

To confront the issue of low-speed maneuverability in the presence of ocean currents and near-shore obstacles, flapping fin mechanisms have been studied to understand

how certain aquatic animals achieve their high levels of controllability. Blake [1] determined that in low-speed operations, labriform motion (using pectoral fin oscillation) is more efficient for maneuvering than carangiform motion (using body and caudal fin undulation). This result indicates that a flapping pectoral fin can be mounted on a rigid UUV hull without sacrificing low-speed maneuverability. Kato et al. [2] and Ando et al. [3] have developed both lift-based and drag-based deformable pectoral fins for use on UUVs. Tangorra et al. [4] have developed a flapping fin based on the bluegill sunfish. They have used CFD simulations and proper orthogonal decomposition analysis to retain the first few modes without replicating the entire fin motion. We have previously carried out 3-D unsteady computations to determine the flow and force production time history of rigid flapping insect wings [5] and flapping and deforming pectoral fins [6]. Those results were compared with and showed good agreement with experimental results. The objectives of this study are to investigate force production of deformable flapping fins and to integrate these fins onto an unmanned underwater vehicle (UUV) capable of superior low-speed maneuverability and hover. Three-dimensional unsteady computations of flapping foil propulsion for bio-inspired UUVs are carried out. The flow past a test vehicle, NRL-UUV, was computed varying the flexibility of the fin, the amplitude of the flapping and starting location of the down stroke. These simulations were performed in order to evaluate the hydrodynamic performance of the vehicle and to assist the controller development of the vehicle. In our previous work, we showed that active control over the curvature of the robotic pectoral fins was necessary to achieve precise low-speed maneuverability of UUVs in highly time-varying external force environments [7]. Design and construction of such a fin, and testing of this fin on a two-fin vehicle have demonstrated the success of this strategy in achieving the force production and vehicle maneuvering capabilities necessary for operation in these challenging environments [8][9].

Licht et al. [10] designed a large (2m × 0.5m × 0.5m) UUV with four rigidly flapping fins with pitch and heave motions and studied pitch biasing as an effective method of vehicle control at hover. In this research effort, we

describe the development of a four-fin vehicle capable of carrying a larger payload, and able to operate at higher forward speed with better pitch control and turning characteristics compared to our two-fin demonstration vehicle. Several cross sections were considered and based on the minimum drag a nearly elliptical cross-section with a smooth leading and trailing sections was obtained. The hydrodynamic characteristics of a newly built prototype vehicle at NRL consisting of four fins were computed for a range of operational conditions and a dynamic mode of this vehicle was created for the development of a controller. Detailed parametric studies were carried out varying several physical and kinematic parameters, such as separation of the two fins, the phasing of the rear fin with respect to the front fin, the stroke amplitudes of the fins, to mention a few. The kinematics corresponding to the fin producing a forward thrust was used to perform parametric studies for a vehicle moving at 1kt. The 3-D unsteady flow solver is coupled to a 6-dof model to simulate a yaw maneuver of the vehicle using different kinematics for the right and left fins. The computational results are obtained using an unstructured grid based Navier-Stokes solver, *feslo*, which is briefly described next.

## II. Incompressible Flow Solver

The governing equations employed are the incompressible Navier-Stokes equations in Arbitrary Lagrangian-Eulerian (ALE) formulation which are written as

$$\frac{d\mathbf{v}}{dt} + \mathbf{v}_a \cdot \nabla \mathbf{v} + \nabla p = \nabla \cdot \sigma \quad (1)$$

$$\nabla \cdot \mathbf{v} = 0 \quad (2)$$

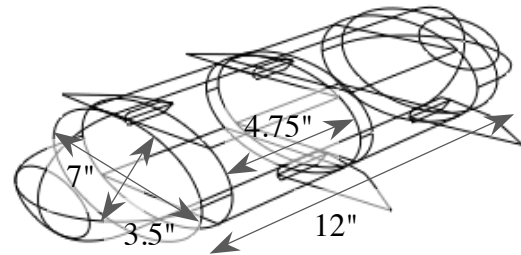
where  $p$  denotes the pressure,  $\mathbf{v}_a = \mathbf{v} - \mathbf{w}$  the advective velocity vector, where  $\mathbf{v}$  is the flow velocity and  $\mathbf{w}$  is the mesh velocity and the material derivative is with respect to the mesh velocity  $\mathbf{w}$ . Both the pressure  $p$  and the stress tensor  $\sigma$  have been normalized by the (constant) density  $\rho$  and are discretized in time using an implicit time stepping procedure. Thus the equations are Eulerian for zero mesh velocity and Lagrangian if the mesh velocity is the same as the flow velocity. The present time-accurate flow solver is discretized in space using a Galerkin procedure with linear tetrahedral elements. The details of the flow solver have already been discussed extensively elsewhere, Ramamurti *et. al.* [6,7], in connection with successfully validated solutions for numerous 2-D and 3-D, laminar and turbulent, steady and unsteady flow problems.

## III. Results and Discussion

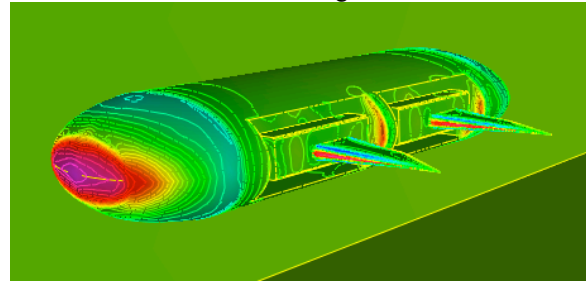
### Vehicle Selection:

Ramamurti *et al.* [7] have computed the unsteady flow past a UUV with flapping fins. Several parametric studies were performed for an isolated flapping fin and were demonstrated using a vehicle that carries two actively controlled curvature fins. In order to carry a larger payload, and to be able to operate at higher forward speed

with better pitch control and turning characteristics compared to our two-fin vehicle, we considered a four-fin vehicle. Several cross sections were considered and the drag was minimized for a flow velocity of 1kt. An elliptical cross section configuration with 3.5" and 7" as the minor and major axes, respectively, and the nose and the tail sections made of elliptical caps, resulted in the minimum drag. The fully extended fins and the boxes that house the servos were then added to the body and the resulting configuration, called the NRL-UUV is shown in Fig. 1a. The overall length of this vehicle is 17.25" and the drag for this configuration is 0.44N. The surface pressure distribution on this configuration at  $V = 1\text{kt}$  is shown in Fig. 1b.



a. vehicle configuration



b. surface pressure distribution

Fig. 1. Flow past NRL-UUV with fins.

The steady flow hydrodynamic characteristics of this configuration is next obtained for a vehicle speed,  $V = 1\text{kt}$ , and for various angles of attack,  $\alpha$ , in the range of  $0^\circ$  to  $30^\circ$  and side slip angle,  $\beta$ , in the range of  $0^\circ$  to  $15^\circ$ . Figure 2 shows the variation of the total lift and drag on the body and fins with pitch angle of attack. The lift force varies linearly and the drag force varies in a quadratic manner with angle of attack, as expected. In order to obtain the hydrodynamic damping coefficients, the vehicle was subjected to a constant turn rate ( $\dot{\gamma}$ ,  $\dot{\beta}$ ,  $\dot{\alpha}$ ) about each of the axes ( $x, y, z$ ), individually. For instance, as the yaw rate  $\dot{\beta}$ , is increased for  $15^\circ$  to  $30^\circ$  per second, the yaw moment  $M_y$ , increases in magnitude nearly four fold from  $2.16\text{E-}04$  to  $8.56\text{E-}04$ . These vehicle hydrodynamic characteristics together with the force production of isolated flapping fins for specific sets of kinematics, called gaits, were incorporated in the development of the vehicle controller.

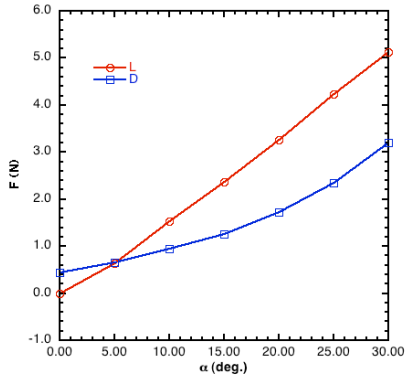


Fig. 2. Variation of lift and drag forces with pitch angle of attack.

### Parametric Studies:

Detailed studies were conducted varying several physical and kinematic parameters, such as the spacing between front and rear fins, phasing of the rear fin with respect to the front, vehicle speed and orientation of the rear fin. These are described next.

### Effect of axial separation of the fins:

Initial studies were conducted to understand the effect of axial separation of the rear fin from the front fin on the thrust and lift production using two isolated, tandem flapping fins. For this study, two separation distances,  $x_{\text{rear}}$  of 3" and 6" were considered. The deforming motion of the flapping fin is obtained by prescribing the motion of five control points located at the tip of the ribs as described in Ramamurti et al. [7]. The kinematics of the ribs is decomposed into a bulk rotation about the fin axis of rotation and a supplemental relative rib rotation, and has a bulk rotation amplitude of  $130^\circ$  at a flapping frequency of 0.91 Hz. The separation between the front and the rear fins was initially set to 6". The computed results for the time history of thrust and lift production show that both thrust and lift production from the rear fin is almost the same as that of the front fin. This suggests that the rear fin is not getting the benefit from the wake resulting from the front fin. Particle traces released near the leading and trailing edges of the front fin show that the resulting wake impinges only a small portion of the fin tip region. Hence, the separation distance was reduced to 3". The thrust and lift production for this case shows only a modest gain in thrust from the rear fin. One reason for this may be due to the fact that the fins are flapping in stagnant water and a positive inflow will be able to carry the wake into the rear fin. The particle traces for these two cases are shown in Fig. 3 suggest that although the wake from the front fin impinges on the rear fin, the phasing may not be optimum.

### Effect of Phasing of the Rear Fin:

Further parametric studies were performed varying the phasing of the rear fin with respect to the front fin and the vehicle speed. For this study, the fins were mounted on the NRL-UUV, described before. The axial separation of the rear fin from the front fin is 4.35". An improved set of kinematics producing forward thrust with the fin flapping

at 1.82 Hz and a reduced bulk amplitude of  $83.3^\circ$  was used for this study and is shown in Fig. 4. Results from the computations on an isolated fin, Fig. 5, show that the mean thrust using this new set at hover is 0.21 N compared to 0.11 N using the previous set of kinematics. As the vehicle velocity is increased to 1kt, the force production from the rear fin is 0.073 N compared to 0.04 N from the front fin as shown in Fig. 5. From this figure, it is clear that after stroke reversals, the rear fin produces additional thrust arising from the wake capture effect. This is similar to the effect that is evidenced in the hovering fruitfly, shown in previous studies by Dickinson et al. [11] and Ramamurti and Sandberg [5].

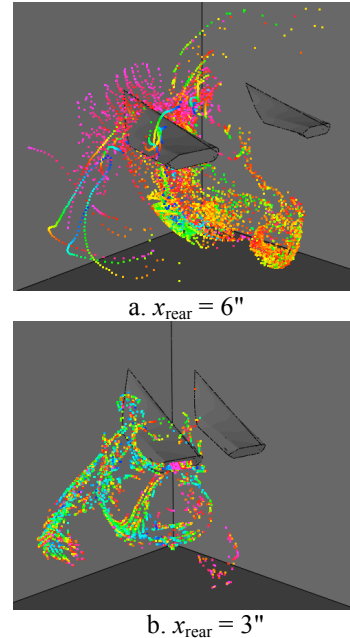
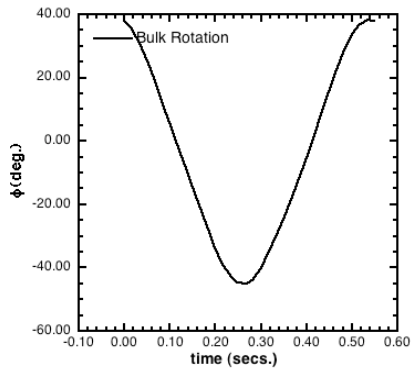
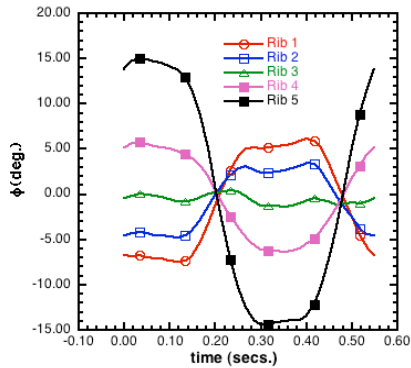


Fig. 3. Particle traces released from the front fin.

This kinematics shown in Fig. 4, was obtained experimentally at 33 time intervals and a flapping frequency of 1.818 Hz. The phasing of the rear fin was modified by altering the starting time interval with respect to the front fin. The shift in time intervals that were chosen are  $\{\pm 2, \pm 4, \pm 8, 17\}$ , resulting in a phase shift of  $\delta = \{\mp 21.8^\circ, \mp 43.6^\circ, \mp 87.3^\circ, -174.6^\circ\}$ , respectively. Unsteady flow computations were performed over these configurations for several flapping cycles, and the results were time averaged over 5 flapping cycles. The variation of the mean thrust from the front and rear fins is shown in Fig. 6. The front fin produces a constant thrust of nearly 0.04N. The rear fin produces 0.073N of mean thrust, a factor of nearly 1.8 times of the front fin when flapped in phase. This mean thrust increases to a value of 0.083N when the phasing is lagged by  $43.6^\circ$ , a factor of nearly 2.1. As the phasing is lagged further, the thrust produced during the mid stroke reduces, resulting in a mean thrust of 0.059N at  $87.3^\circ$  and 0.014N at  $174.6^\circ$ . A phase lead of  $43.6^\circ$  results in a reduced mean thrust of 0.069N. The



a. Bulk rotation



b. Relative rotation

Fig. 4. Kinematics for a flapping deforming fin producing forward thrust,  $f = 1.818\text{Hz}$ .

reason for this additional thrust at  $\delta = -43.6^\circ$ , is due to the capture of the wake that is produced by the front fin. This reduces the loss of thrust just before and after the stroke reversals, as shown in Fig. 7, although the peak thrust at the beginning of the upstroke is reduced. For clarity, only few of the time histories are shown in Fig. 7. When the rear fin leads the front fin by  $43.6^\circ$ , the peak thrust after the stroke reversal is delayed leading to a reduced mean thrust.

The thrust and lift production from the flapping fins when the rear is lagged by  $43.6^\circ$  is shown in Fig. 8. The additional thrust from the rear fin can be analyzed from the surface pressure distribution. Figure 9 shows the surface pressure distribution on the vehicle at  $t = 1.208\text{s}$  when the thrust from the rear fin reaches a maximum after the stroke reversal to the upstroke. The orientation of the front and the rear fins due to the phase lag is shown in this figure. A close look at the pressure distribution on the top and bottom surfaces at this instant, Fig. 10a-d, shows that the pressure in the leading edge region in the top surface of the rear fin, Fig. 10c, is much higher compared to that of the front fin, Fig. 10a. Also, the pressure in the leading edge region on the bottom surface, Fig. 10d is much lower compared to that of the front fin, Fig. 10b. In addition to this, the orientation of the rear fin is such that the net force is directed in the  $x$ -direction. In comparison, the surface pressure distribution on the front fin at the same orientation, at  $t = 1.143\text{s}$ , exhibits a much reduced pressure

on the top surface and higher minimum pressure on the bottom surface of the fin.

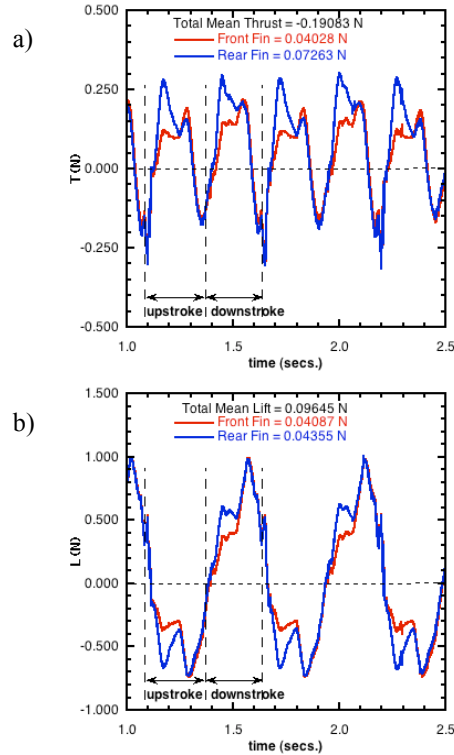


Fig. 5. Thrust and lift production from tandem flapping fins,  $f = 1.818\text{Hz}$ ,  $V = 1\text{kt}$ .

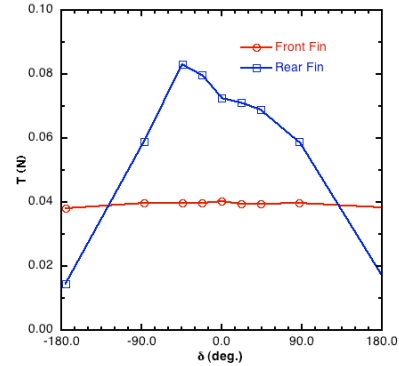


Fig. 6. Variation of Mean thrust with phasing of the rear fin,  $V = 1\text{kt}$ .

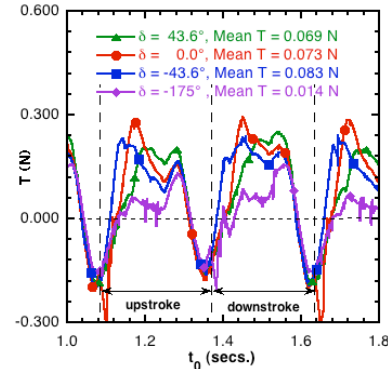


Fig. 7. Effect of phasing on the time history of thrust produced by the rear fin,  $V = 1\text{kt}$ .

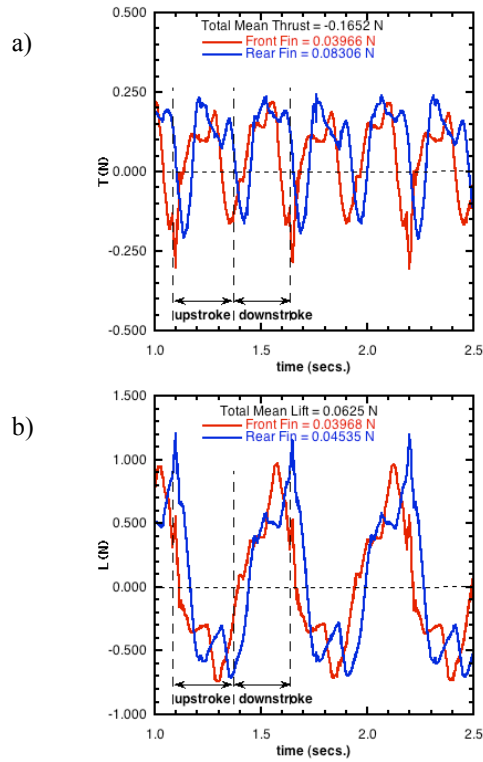


Fig. 8. Thrust and lift production from tandem flapping fins,  $f = 1.818\text{Hz}$ ,  $V = 1\text{kt}$ ,  $\delta = -43.6^\circ$ .

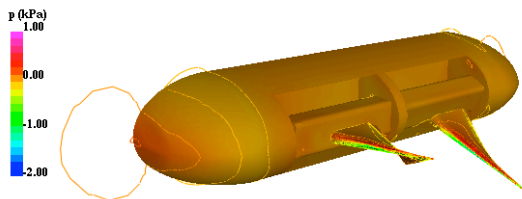
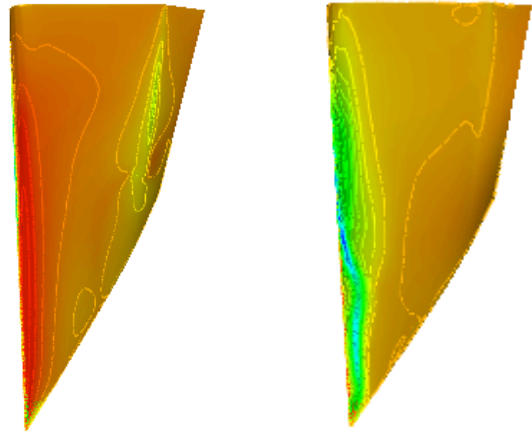
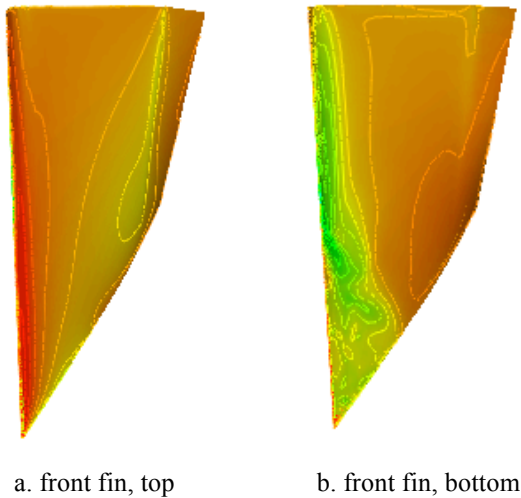


Fig. 9. Surface pressure distribution on NRL-UUV at  $t = 1.208\text{s}$ ,  $V = 1\text{kt}$ ,  $\delta = -43.6^\circ$ .



c. rear fin, top  
d. rear fin, bottom  
Fig. 10. Surface pressure distribution on the flapping fins,  $t = 1.208\text{s}$ .

**Effect of Vehicle Speed:**

The effect of the incoming flow velocity on the thrust and lift production was tested on an isolated fin flapping according to the kinematics described in Fig. 4. As the flow velocity is increased from 0kts to 1kt, the mean thrust produced by the fin reduces from 0.21N to 0.04N, as shown in Fig. 11a; the mean thrust at 0.5kts is nearly 0.12N. The mean lift also increases from 0.017N to 0.04N, Fig. 11b.

Since, the parametric studies varying the phasing of the rear fin showed that the rear fin produces the maximum thrust compared to the front fin at  $\delta = -43.6^\circ$ , further

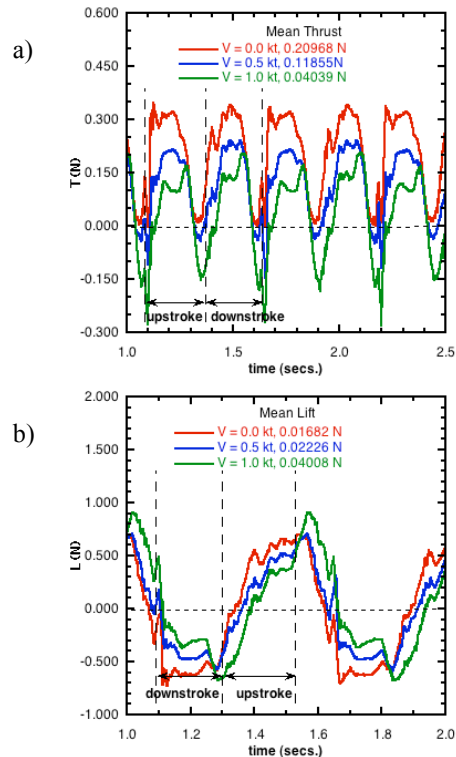


Fig. 11. Effect of inflow velocity on thrust and lift production from a single flapping fin.

studies varying the vehicle speed were performed at this phase. The time history of the thrust produced by the front and rear fins are shown in Fig. 12. At hover, the thrust produced by the front and rear fins are identical and are positive throughout the stroke. As the vehicle speed is increased to 0.25kts, the maximum thrust produced in the midstroke is reduced. Also, the peak thrust produced just after the stroke reversal, due to the wake capture effect, is also reduced. As the vehicle speed is increased further, the thrust produced in the midstroke reduces, and the fin produces a drag around stroke reversal for the front fin, Fig. 12a, and just after stroke reversal, Fig. 12b, for the rear fin. At a vehicle speed of 1kt, the thrust produced by the rear fin exhibits a larger peak after stroke reversal, (black line in Fig. 12b), compared to that of the front fin, Fig. 12a, thus producing a higher mean thrust.

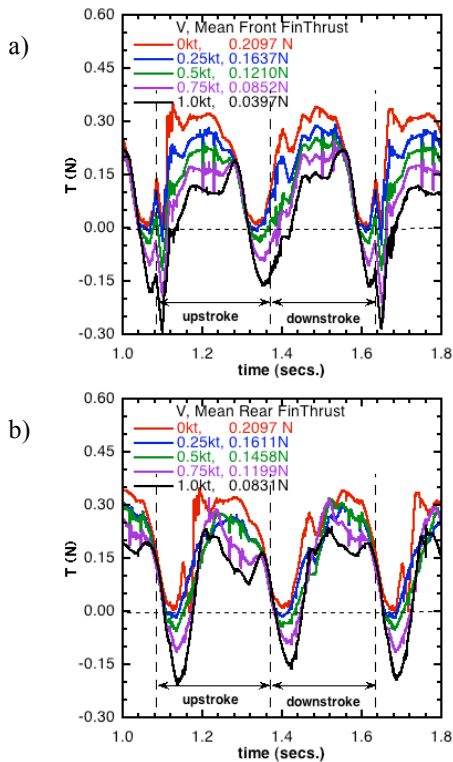


Fig. 12. Variation of unsteady thrust production from the flapping fins with vehicle speed, a) front fin and b) rear fin.

Figure 13a, shows the thrust produced by the front and rear fins, the drag on half the body from steady state computations at  $\alpha = 0^\circ$ , and the total thrust on the vehicle from unsteady computations. From the thrust balance between the total fin thrust and the steady state drag, the vehicle should be able to maintain a forward speed of nearly 0.9kts. The interaction of the flapping fin and the servo boxes with the body produced additional drag on the vehicle. Hence, from the mean thrust of the unsteady simulations it is clear that the vehicle can maintain nearly 0.8kts of forward speed. This forward speed is only slightly higher than our previous two fin vehicle speed of 0.66kts, mainly due to the larger drag on the vehicle. As

the vehicle speed is increased from hover to  $V=1$ kt, the rear fin produces more than double the thrust produced by the front fin, shown in Fig. 13b. The reason for this is due to the stronger wake capture effect after stroke reversals for the rear fin, and the effect of the oncoming flow from the wake of the front fin. The flow just upstream of the front and the rear fins are very different, as shown in Fig. 14, at two planes,  $x = 2.0''$  and  $6.0''$ , just ahead of the leading edges of the fins. The magnitude of velocity, Fig. 14a, shows a high velocity region (magenta), in the mid chord of the rear fin and a wake region (blue) towards the wing tip region. This is also clear in the streamwise component of vorticity contours shown in Fig. 14b. Due to these changes in the incoming flow conditions, the wake capture effect of the rear fin is strengthened and leads to the additional thrust. Figure 15 shows the spanwise component of vorticity at  $z = 6.5''$ , for the front and rear fins. It is clear that the vortex that is formed on the rear fin is much stronger compared to that on the front fin, leading to a lower pressure on the bottom surface of the rear fin, and thus producing a higher thrust.

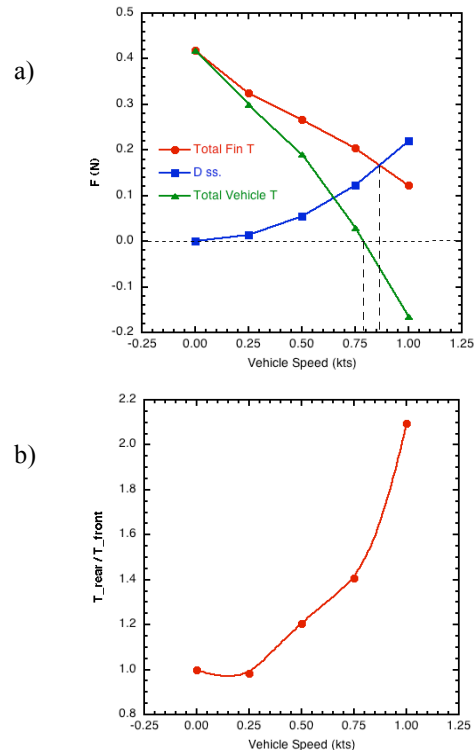


Fig. 13. Effect of vehicle speed on the mean thrust produced by the fins, a) Net mean thrust and b) ratio of the mean thrusts.

#### Yaw Maneuver:

In order to simulate a yaw turn of the vehicle, the set of kinematics producing forward thrust, Fig 4, is used for the left side fins, while a set of kinematics that produces a reverse thrust, Fig. 16, is used for the right side fins scaled to match the frequency of the front fin. The flow past an isolated fin flapping with this set of kinematics was first simulated. The bulk rotation for this set is similar to that

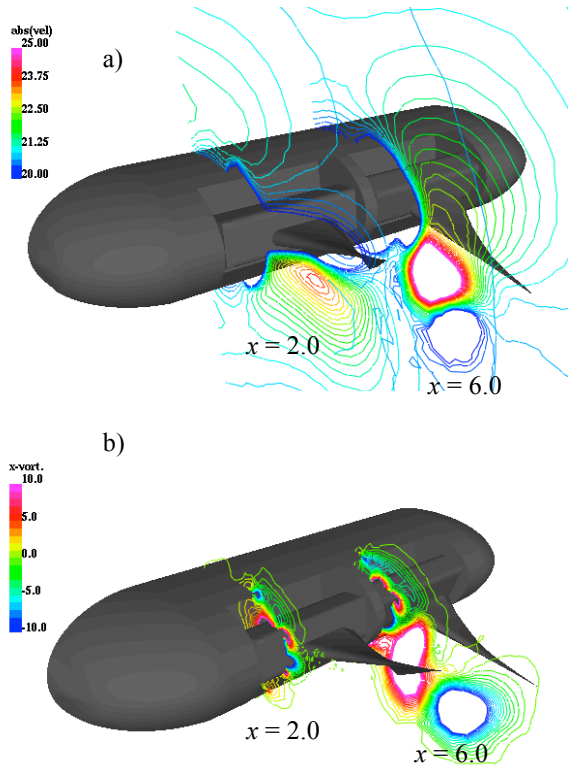


Fig. 14. Inflow conditions for the front and rear fins at  $t = 1.208s$ ,  $V = 1kt$ ,  $\delta = -43.6^\circ$ , a) magnitude of velocity and b) streamwise component of vorticity.

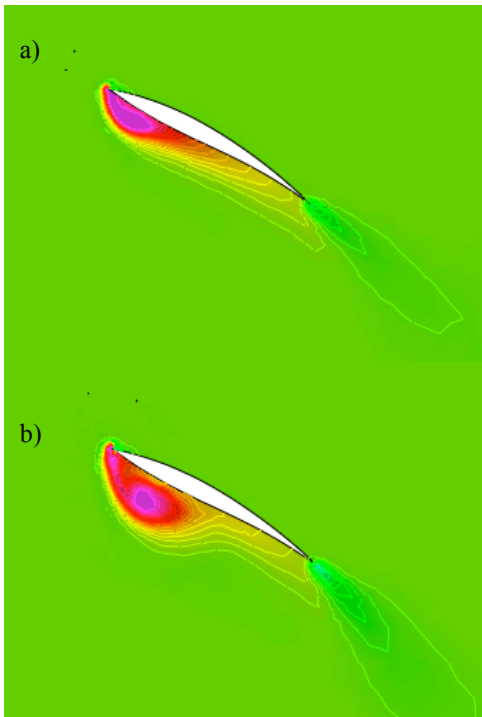


Fig. 15. Spanwise component of vorticity at  $z = 6.5''$ ,  $V = 1kt$ ,  $\delta = -43.6^\circ$ , a. front fin,  $t = 1.143s$ , b. rear fin,  $t = 1.208s$ .

of the forward thrust producing kinematics. The relative rotations of the ribs are reversed compared to Fig. 4b, and rib 5 leads rib 1 throughout the flapping cycle. With the fin flapping at  $1.765Hz$ , a mean thrust of nearly  $-0.14N$  is produced and the mean lift produced is nearly zero. As the mean reverse thrust is smaller compared to the mean forward thrust produced by the kinematics,  $0.21N$ , the relative rotations of the forward gait, Fig. 4b, were halved. This is based on our previous study, Ramamurti et al [7], on varying the flexibility of the fin past an isolated flapping fin.

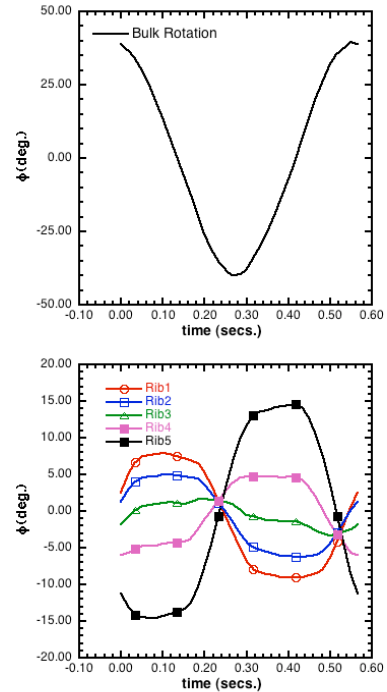


Fig. 16. Kinematics for a flapping deforming fin producing reverse thrust,  $f = 1.765Hz$ .

For the yaw maneuver simulation, the complete vehicle with four flapping fins was considered, and the net forces and moments were computed. The mesh that was employed for the simulation consists of  $1.9M$  points and  $10.7M$  tetrahedral elements. In this initial simulation the vehicle was held in place with all the 4 fins flapping. The time history of forces and moments produced are shown in Fig. 17. The mean thrust produced by the left and the right fins are  $-0.41N$  and  $0.34N$ , respectively, Fig. 17a; the mean total thrust and lift on the vehicle are  $-0.07N$  and  $0.068N$ , Figs. 17b and c. The mean side force on the vehicle is nearly  $0.02N$ , Fig. 17d. The mean yaw moment produced by the left and right fins are  $0.058N\cdot m$  and  $0.045N\cdot m$ , respectively, Fig. 17e and the mean total yaw moment on the vehicle is  $0.103N\cdot m$ , Fig. 17f. The mean pitch and the roll moments are nearly zero.

Next, the vehicle was unconstrained in the yaw degree of freedom, while all the other degrees of 6-dof model were constrained. For this simulation, the moment of inertia of the yaw axis of the vehicle through the center of gravity was computed both from the volume representation

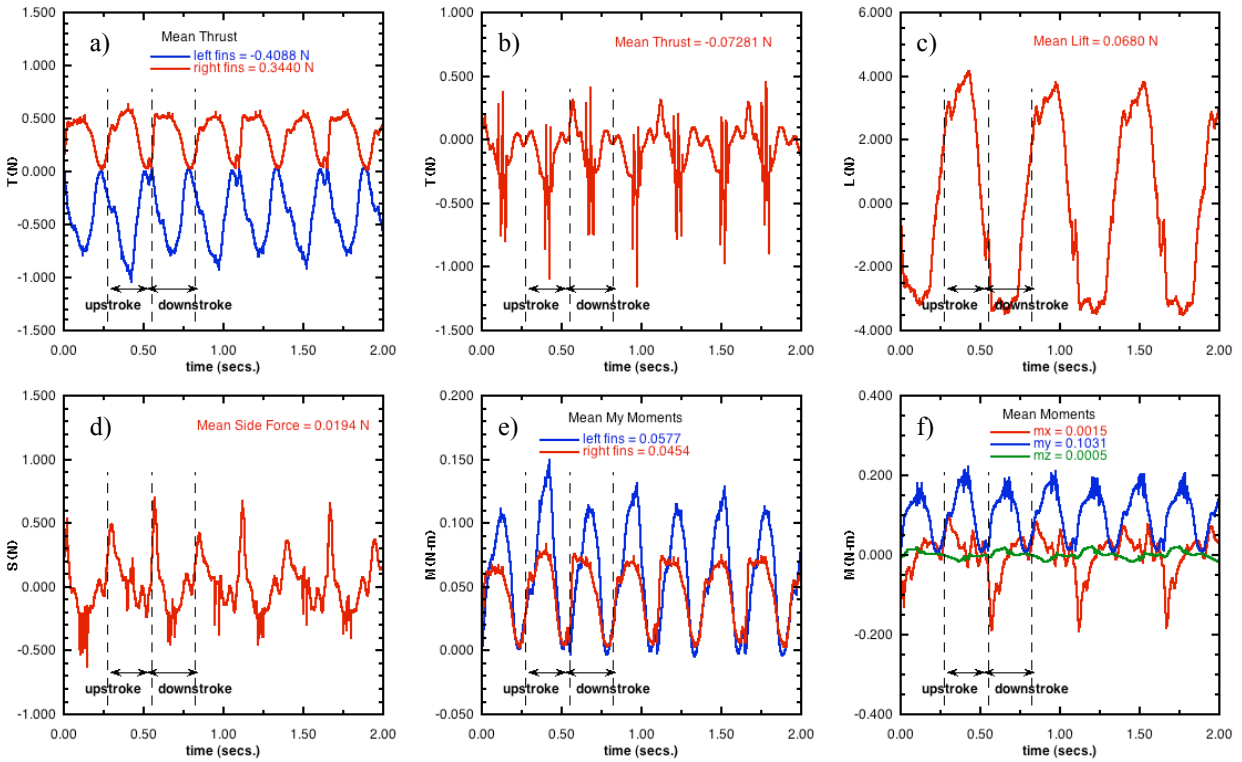


Fig. 17. Forces and moments on the NRL-UUV, a) Fin Thrust, b) Total Thrust, c) Total Lift, d) Total Side Force, e) Fin Yaw Moment, and f) Total Moments.

in the simulations and from the actual vehicle geometry, and are  $0.0483\text{Kg}\cdot\text{m}^2$  and  $0.0262\text{Kg}\cdot\text{m}^2$ . For the maneuvering simulations, the value from the actual vehicle geometry was used. The total force and moment time history on the vehicle is shown in Fig. 18. The force time history, Fig. 18a, shows that the mean thrust and side forces are nearly zero and that the vertical force exhibits a larger range of variation. The moment time history, Fig. 18b, shows that the yaw moment,  $M_y$ , remains positive for the entire maneuver and the pitch moment despite having a larger range of values has a nearly zero mean moment. The yaw rate and the yaw turn angle of the vehicle are shown in Fig. 19. It is clear that the vehicle completes a full turn in nearly 2.5s. The yaw turn rate shows an oscillatory behavior arising from the total yaw moment on the vehicle and achieves an asymptotic value of nearly  $180^\circ/\text{s}$ . This turn rate is higher than that was observed in the experiments which has a maximum rate of  $40^\circ/\text{s}$ . The discrepancy may be due to the moment of inertia that is used in the simulation which is nearly half that is based on volume, and the kinematics that were employed in the simulation that are different from the experiments. Hence, the experimental kinematics have to be obtained and will be used in the future simulations for comparison.

#### Effect of Fin Orientation:

Another method of rapidly making a  $180^\circ$  turn is to make the vehicle symmetric front to back by orienting the rear fins such that the longer leading edge faces the rear of the vehicle, as shown in Fig. 20. In this case, the

kinematics for the front and rear fins can be swapped to enable a quick reverse thrust on the vehicle. For these simulations, the fins that are facing the free stream velocity are termed the front fins. First, simulations were

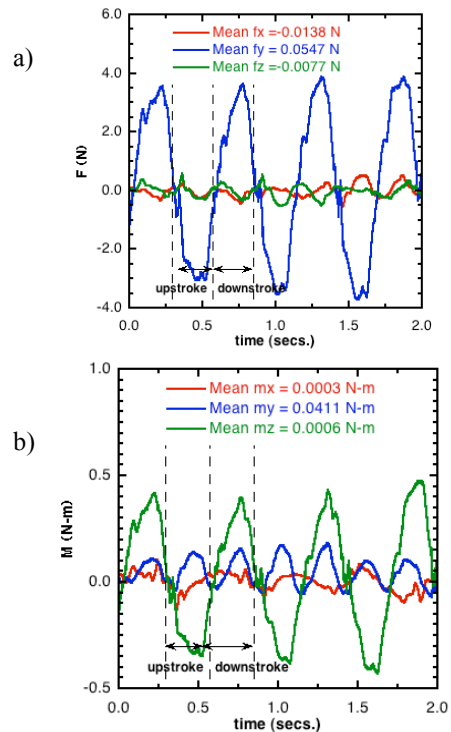


Fig. 18. Forces and moments on the NRL-UUV undergoing a yaw maneuver, a) Total Forces and b) Total Moments.

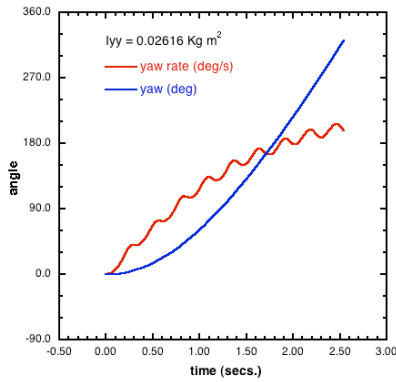


Fig. 19. Trajectory of NRL-UUV during a yaw turn.

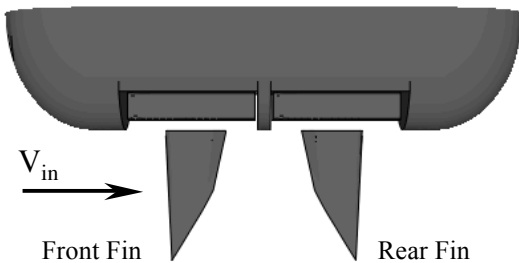


Fig. 20. Vehicle configuration with symmetric fin orientation.

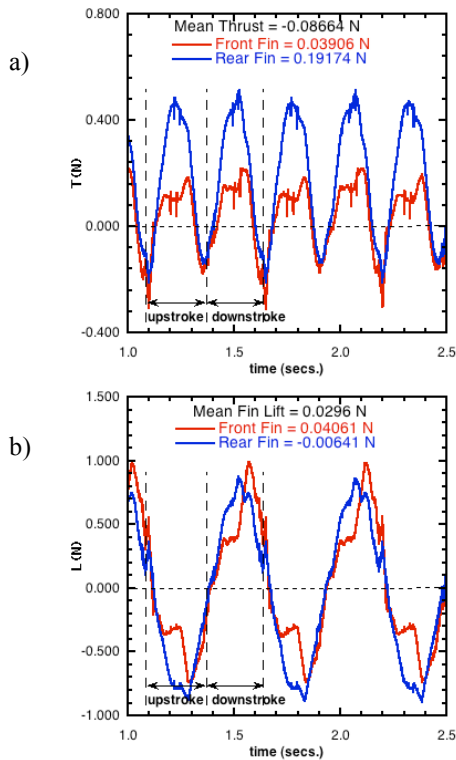


Fig. 21. Thrust and lift production for a vehicle with symmetric fin orientation, front fin with forward thrust kinematics and rear fin with reverse thrust kinematics,  $V = 1\text{kt}$ .

performed for this configuration with the front fins using the forward thrust gait, Fig. 4, and the rear fins using a reverse thrust gait, Fig. 16. Figure 21 shows the thrust and lift generated in this configuration at a vehicle speed of 1kt. It is clear that the rear fin produces nearly 5 times the thrust of the front fin, compared to nearly twice when the rear fin is oriented forward and using the forward thrust kinematics. The total drag on the vehicle is 0.087N. The lift produced by the rear fin is reduced to nearly zero compared to 0.045N, Fig. 8b. In this configuration the vehicle will be able to maintain a forward speed of 0.88kts. The reason for the increased thrust from the rear fin is mainly due to the selected kinematics and the orientation of the rear fin in the oncoming wake of the front fin as shown in Fig. 22. High pressure region extends on most of the top surface of the rear fin, Fig. 22b, while the fin is tilted forwards. At this instant, although the front fin has a similar orientation, Fig. 22a, the surface pressure on the top surface, Fig. 22d, is much reduced.

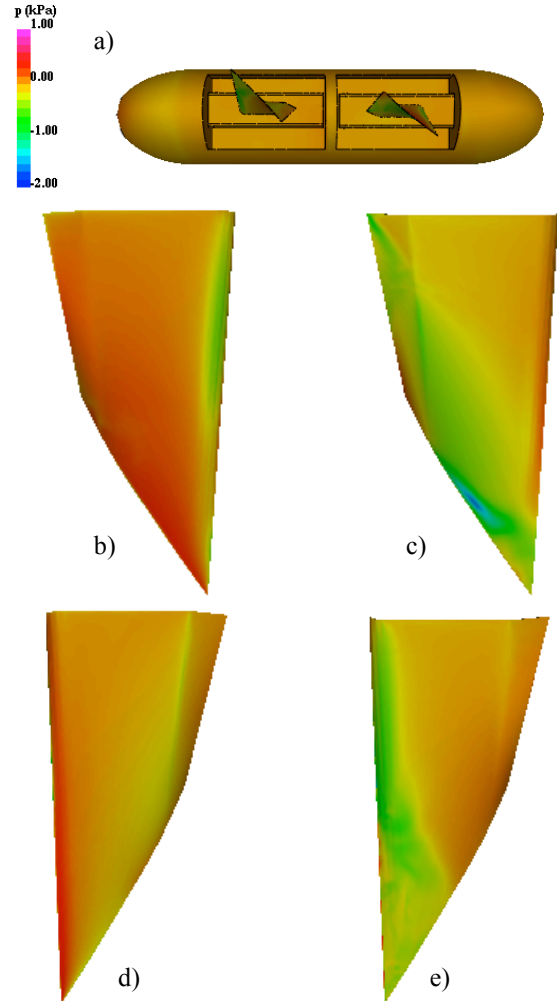


Fig. 22. Surface pressure distribution on vehicle with symmetric fin orientation,  $t = 1.215\text{s}$ ,  $V = 1\text{kt}$ , a) side view showing fin orientation, b) rear fin, top, c) rear fin, bottom, d) front fin, top and e) front fin, bottom.

All possible combinations of kinematics for the front and the rear fins with forward and reverse thrust kinematics were simulated at both 0.5kts and 1kt vehicle speed. In terms of reverse thrust, the combination of using forward thrust kinematics for the front and rear fins, produced a reverse thrust of nearly 0.77N at 1kt vehicle speed; the combination of reverse thrust for the front fin and forward thrust for the rear fin produced 0.67N of reverse thrust. At a lower vehicle speed of 0.5kts, the latter combination produces slightly more reverse thrust of 0.38N compared to the former combination of 0.3N. Hence, the latter combination using reverse thrust for the front fin and forward thrust for the rear fin can be used to quickly decelerate the vehicle and reverse to avoid obstacles. A yaw maneuver in this configuration will use the combination of forward thrust for the front fin and reverse thrust for the rear fin on the right side of the vehicle and the anti-symmetric combination on the left side of the vehicle. Further maneuvering simulations will be conducted using the experimental kinematics used for the turning maneuver in order to compare the turning rate and the trajectory.

## SUMMARY

The 3-D unsteady computations past a UUV with four actively controlled curvature fins were carried out. Several cross sections of the vehicle were considered and based on the minimum drag an elliptical cross section was chosen. Hydrodynamic characteristics of the vehicle for various angles of attack, side slip angles, and turn characteristics were simulated and were incorporated in the dynamic modeling of the vehicle. Parametric studies varying the spacing between the front and rear fins showed that the wake capture effect was not pronounced at hover, but is significant as the vehicle speed increased. At a vehicle speed of 1kt, the rear fins produce nearly 1.8 times the thrust as that of the front fins, and improve further to a factor of 2.1 when they are lagged in phase by nearly 44°. The mean thrust from the unsteady simulations showed that the vehicle was able to maintain a forward speed of nearly 0.8kts. The unsteady flow solver with flapping deforming fins was coupled to a 6-dof trajectory model and was tested to simulate a yaw turn. The results showed that the vehicle turning rate was nearly 180°/s. The effect of fin orientation was studied by making the vehicle symmetric front to back and using various combinations of forward and reverse thrust producing kinematics. It was found that using forward thrust kinematics for the front fin and reverse thrust kinematics for the rear fin produced enough thrust to maintain a velocity of nearly 0.9kts. Further maneuvering simulations will be performed with this configuration of the vehicle using experimental kinematics, and the trajectories will be compared.

## ACKNOWLEDGEMENTS

This work was supported by ONR through an NRL 6.2 project: "Unsteady Hydrodynamics of Swimming Vehicles." The valuable discussions with Prof. Rainald

Löhner of George Mason University are greatly appreciated. This work was supported in part by a grant of HPC time from the DoD HPC center for the NRL SGI-Altix.

## REFERENCES

1. Blake R.W., "The mechanics of labriform motion I. Labriform locomotion in the angelfish (*pterophyllum eimekei*): An analysis of the power stroke", *J. Exp. Biol.*, **82**, 1979, pp. 255-271.
2. Kato, N., Liu, H. and Morikawa, H., "Biology-Inspired Precision Maneuvering of Underwater Vehicles," *Proc. of the 12<sup>th</sup> Intl. offshore and Polar Engg. Conf.*, Vol. 2, 2002, pp. 269-276.
3. Ando, Y., Kato, N., Suzuki, H., Ariyoshi, T., Suzumori, K., Kanda, T. and Endo, S., "Elastic Pectoral Fin Actuators for Biomimetic Underwater Vehicles," *Proc. of the 16<sup>th</sup> Intl. offshore and Polar Engg. Conf.*, 2006, pp. 260-267.
4. Tangorra, J.L., Davidson, S. N., Hunter, I., Madden, P.G.A., Lauder, G.V., Dong, H., Bozukurttas, M. and Mittal, R., "The Development of a Biologically Inspired Propulsor for Unmanned Underwater Vehicles," *IEEE J. of Ocean Engg.*, Vol. 32, No. 3, July 2007, pp. 533-550.
5. Ramamurti, R. and Sandberg, W.C., "A 3-D Computational Study of the Aerodynamic Characteristics of Insect Flight," *J. exp. Biology*, Vol. 205, No. 10, pp. 1507-1518, May 2002.
6. Ramamurti, R., Sandberg, W.C., Löhner, R., Walker, J.A. and Westneat, M.M., "Fluid Dynamics of Flapping Aquatic Flight in the Bird Wrasse: 3-D Unsteady Computations with Fin Deformation," *J. exp. Biology*, Vol. 205, No. 19, pp. 2997-3008, October 2002.
7. Ramamurti, R., Geder, J.D., Palmisano, J., Ratna, B. and Sandberg, W.C., "Computations of Flapping Flow Propulsion for Unmanned Underwater Vehicle Design," *AIAA J.*, Vol. 48, No. 1, pp. 188-201, January 2010.
8. Palmisano, J., Ramamurti, R., Lu, K.J., Cohen, J., Sandberg, W. C. and Ratna, B., "Design of a Biomimetic Controlled-Curvature Robotic Pectoral Fin," *2007 IEEE Int. Conf. on Robotics and Automation*, Roma, Italy.
9. Geder, J., Ramamurti, R., Palmisano, J., Pruessner, M., Ratna, B. and Sandberg, W. C., "Sensor Data Fusion and Submerged Test Results of a Pectoral Fin Propelled UUV," *16th International Symposium on Unmanned Untethered Submersible Technology*, Durham, New Hampshire, USA, August 23-26, 2009.
10. Licht, S., Polidoro, V., Flores, M. and Hover, F.S., "Design and Projected Performance of a Flapping Foil AUV," *IEEE J. of Ocean Engg.*, Vol. 29, No. 3, July 2004.
11. Dickinson, M. H., Lehmann, F.-O. and Sane, S. P., "Wing rotation and the aerodynamic basis of insect flight," *Science*, Vol. 284, 1999, pp. 1954-1960.